



HAL
open science

BRCA1-methylated triple negative breast cancers previously exposed to neoadjuvant chemotherapy form RAD51 foci and respond poorly to olaparib

Carolina Velazquez, Esin Orhan, Imene Tabet, Lise Fenou, Béatrice Orsetti, José Adélaïde, Arnaud Guille, Simon Thézénas, Evelyne Lopez-Crapez, Pierre-Emmanuel Colombo, et al.

► To cite this version:

Carolina Velazquez, Esin Orhan, Imene Tabet, Lise Fenou, Béatrice Orsetti, et al.. BRCA1-methylated triple negative breast cancers previously exposed to neoadjuvant chemotherapy form RAD51 foci and respond poorly to olaparib. *Frontiers in Oncology*, 2023, 13, pp.1125021. 10.3389/fonc.2023.1125021 . hal-04275543

HAL Id: hal-04275543

<https://hal.science/hal-04275543>

Submitted on 5 Apr 2024

HAL is a multi-disciplinary open access archive for the deposit and dissemination of scientific research documents, whether they are published or not. The documents may come from teaching and research institutions in France or abroad, or from public or private research centers.

L'archive ouverte pluridisciplinaire **HAL**, est destinée au dépôt et à la diffusion de documents scientifiques de niveau recherche, publiés ou non, émanant des établissements d'enseignement et de recherche français ou étrangers, des laboratoires publics ou privés.



OPEN ACCESS

EDITED BY

Chunyan Dong,
Tongji University, China

REVIEWED BY

Federica Guffanti,
Mario Negri Institute for Pharmacological
Research (IRCCS), Italy
Guang Peng,
University of Texas MD Anderson Cancer
Center, United States
Yinlong Yang,
Fudan University, China
Pete Simpson,
The University of Queensland, Australia

*CORRESPONDENCE

Charles Theillet
✉ charles.theillet@inserm.fr

[†]These authors have contributed equally to
this work

SPECIALTY SECTION

This article was submitted to
Breast Cancer,
a section of the journal
Frontiers in Oncology

RECEIVED 15 December 2022

ACCEPTED 03 March 2023

PUBLISHED 17 March 2023

CITATION

Velazquez C, Orhan E, Tabet I, Fenou L,
Orsetti B, Adélaïde J, Guille A, Thézénas S,
Crapez E, Colombo P-E, Chaffanet M,
Birnbaum D, Sardet C, Jacot W and
Theillet C (2023) *BRCA1*-methylated triple
negative breast cancers previously exposed
to neoadjuvant chemotherapy form RAD51
foci and respond poorly to olaparib.
Front. Oncol. 13:1125021.
doi: 10.3389/fonc.2023.1125021

COPYRIGHT

© 2023 Velazquez, Orhan, Tabet, Fenou,
Orsetti, Adélaïde, Guille, Thézénas, Crapez,
Colombo, Chaffanet, Birnbaum, Sardet, Jacot
and Theillet. This is an open-access article
distributed under the terms of the [Creative
Commons Attribution License \(CC BY\)](#). The
use, distribution or reproduction in other
forums is permitted, provided the original
author(s) and the copyright owner(s) are
credited and that the original publication in
this journal is cited, in accordance with
accepted academic practice. No use,
distribution or reproduction is permitted
which does not comply with these terms.

BRCA1-methylated triple negative breast cancers previously exposed to neoadjuvant chemotherapy form RAD51 foci and respond poorly to olaparib

Carolina Velazquez^{1†}, Esin Orhan^{1†}, Imene Tabet¹, Lise Fenou¹,
Béatrice Orsetti¹, José Adélaïde², Arnaud Guille²,
Simon Thézénas³, Evelyne Crapez⁴,
Pierre-Emmanuel Colombo^{1,5}, Max Chaffanet²,
Daniel Birnbaum², Claude Sardet¹,
William Jacot^{1,6} and Charles Theillet^{1*}

¹Institut de Recherche en Cancérologie de Montpellier, IRCM U1194, Montpellier University, INSERM, ICM, CNRS, Montpellier, France, ²Centre de Recherche en Cancérologie de Marseille, CRCM UMR1068, Aix-Marseille University, IPC, CNRS, Marseille, France, ³Biometry Unit, Institut du Cancer de Montpellier, Montpellier, France, ⁴Unité de Recherche Translationnelle, Institut du Cancer de Montpellier, Montpellier, France, ⁵Oncological Surgery, Institut du Cancer de Montpellier, Montpellier, France, ⁶Clinical Oncology, Institut du Cancer de Montpellier, Montpellier, France

Background: About 15% of Triple-Negative-Breast-Cancer (TNBC) present silencing of the *BRCA1* promoter methylation and are assumed to be Homologous Recombination Deficient (HRD). *BRCA1*-methylated (*BRCA1*-Me) TNBC could, thus, be eligible to treatment based on PARP-inhibitors or Platinum salts. However, their actual HRD status is discussed, as these tumors are suspected to develop resistance after chemotherapy exposure.

Methods: We interrogated the sensitivity to olaparib vs. carboplatin of 8 TNBC Patient-Derived Xenografts (PDX) models. Four PDX corresponded to *BRCA1*-Me, of which 3 were previously exposed to NeoAdjuvant-Chemotherapy (NACT). The remaining PDX models corresponded to two *BRCA1*-mutated (*BRCA1*-Mut) and two *BRCA1*-wild type PDX that were respectively included as positive and negative controls. The HRD status of our PDX models was assessed using both genomic signatures and the functional *BRCA1* and RAD51 nuclear foci formation assay. To assess HR restoration associated with olaparib resistance, we studied pairs of *BRCA1* deficient cell lines and their resistant subclones.

Results: The 3 *BRCA1*-Me PDX that had been exposed to NACT responded poorly to olaparib, likewise *BRCA1*-WT PDX. Contrastingly, 3 treatment-naïve *BRCA1*-deficient PDX (1 *BRCA1*-Me and 2 *BRCA1*-mutated) responded to olaparib. Noticeably, the three olaparib-responsive PDX scored negative for *BRCA1*- and RAD51-foci, whereas all non-responsive PDX models, including the 3 NACT-exposed *BRCA1*-Me PDX, scored positive for RAD51-foci. This

suggested HRD in olaparib responsive PDX, while non-responsive models were HR proficient. These results were consistent with observations in cell lines showing a significant increase of RAD51-foci in olaparib-resistant subclones compared with sensitive parental cells, suggesting HR restoration in these models.

Conclusion: Our results thus support the notion that the actual HRD status of *BRCA1-Me* TNBC, especially if previously exposed to chemotherapy, may be questioned and should be verified using the *BRCA1*- and *RAD51*-foci assay.

KEYWORDS

TNBC, *BRCA1* methylation, *RAD51*, nuclear foci, HRD (homologous recombination deficiency)

Background

Triple-negative breast cancers (TNBCs) represent 15% of all breast cancers and its most aggressive subtype (1, 2). Despite good initial chemosensitivity, these tumors show early relapse (1, 3) and, until recently, in the absence of validated drugs only a minority of TNBC were eligible for targeted therapies, thus, stressing the need to develop novel approaches (4).

Another interesting characteristic of TNBC is that this subtype comprises the largest fraction of *BRCA* deficient breast tumors (5, 6). *BRCA* deficiency was originally shown to result from coding mutations affecting the *BRCA1* or *BRCA2* genes, which are the principal determinants of genetic predisposition to breast and ovarian cancers and play central role in Homologous Recombination (HR) Repair, also called *BRCA* pathway (7). HR is an essential and accurate DNA repair pathway (7, 8) and, noticeably, tumors with an HR deficiency (HRD) show elevated genetic instability (9) and accrued sensitivity to DNA cross linking agents such as platinum salts (10, 11). Accordingly, it has been proposed to include platinum in the standard of care of TNBC (12). Furthermore, over the past decade, it has been demonstrated that breast tumors with germline *BRCA1* or *BRCA2* mutations are exquisitely sensitive to PARP inhibitors, as part of a synthetic lethal interaction (13–16).

While germline *BRCA1* or *BRCA2* mutations have, until recently, been the only validated indications for PARPi-based therapy in breast and ovarian cancer, it has become clear that they were not the sole causes of an HRD phenotype. Indeed, HRD has also been associated with somatic mutations and/or epigenetic silencing affecting the *BRCA1* and *BRCA2* genes, as well as other genes in the pathway, such as *PALB2*, *RAD51B*, *RAD51C* or *RAD51D* (5, 6). Because of their obvious clinical implications, the questions of the actual number of TNBC presenting HRD and the best approach to detect them have drawn increasing attention. Whole Genome Sequencing of large cohorts of breast and ovarian cancers have revealed that *BRCA*-deficient tumors presented specific patterns of genomic rearrangements, corresponding to scars left behind in the tumor genome by faulty repair (17).

Different genomic signatures (HRDetect, HRD-score, Tandem Duplicator Phenotype, copy number signatures) were established and used to stratify TNBCs and ovarian cancers (17–20). Some of these signatures showed strong association with *BRCA1/2* mutations (germline or somatic), as well as epigenetic silencing of *BRCA1* (17–19, 21). Consequently, the fraction of TNBC with an HRD phenotype, which initially was estimated to range 2.7–17.5% (22, 23), when only germline *BRCA1/2* mutations were taken into account, raised up to 35% on the basis of genomic signatures (17–19, 21). Interestingly, tumors with an HRD genomic profiles were associated with better response to therapy and a more favorable disease outcome (24–27).

Hence, the extension of current PARPi-based therapy indications in TNBC beyond patients bearing germline *BRCA1/2* mutations has become a major question. In particular, the actual sensitivity of tumors with epigenetically silenced *BRCA1* gene due to the hypermethylation of its promoter is of particular interest, as they represent an appreciable 15 to 20% of TNBC (19, 21, 28), but has led to conflicting conclusions (27, 29–32). In particular, the actual *BRCA*-deficiency of post-treatment residual *BRCA1*-hypermethylated tumors and their subsequent recurrences has been questioned (31). This point concurs with observations made in different model systems showing that *BRCA*-deficient tumors rapidly acquire treatment resistance and, in most cases, resistance is due to the partial or complete restoration of HRR upon exposure to either platinum or PARPi (33, 34). Thus, the actual sensitivity of TNBC showing all signs of HRD and, particularly, those with *BRCA1* hypermethylation that have been previously exposed to chemotherapy in the course of the disease could be questioned (31, 35).

To this aim, we tested in the present study the sensitivity of 8 PDX models, comprising 7 TNBC (2 *BRCA1-WT*, 4 *BRCA1*-methylated (*BRCA1-Me*), 1 *BRCA1-Mut*) and 1 *BRCA1-Mut* High Grade Ovarian Serous Ovarian Carcinoma (HGSOC), to the PARP inhibitor olaparib and to carboplatin (CBP). Of the 8 PDX models tested, 3 showed stable disease (SD), while the 5 others progressed under olaparib. PDX models that responded to olaparib were all treatment naïve and corresponded to 2 *BRCA1*-mutated and one

BRCA1-methylated PDX. The five non-responsive PDX comprised 2 *BRCA1* wild type and 3 *BRCA1*-methylated that, noticeably, were established from TNBC tumors that responded poorly to neoadjuvant chemotherapy (NACT). We, thus, interrogated the HRD status of the tested PDX models and used *BRCA1*, *RAD51*, γ H2AX and 53BP1 nuclear foci in olaparib treated PDX as read-outs of HR functionality and of DNA damage response. PDX models with reduced *BRCA1* and *RAD51* foci formation corresponded to olaparib responders, whereas non-responders were all *RAD51*-foci positive. Remarkably, the three *BRCA1-Me* PDX established from tumors that responded poorly to NACT were *RAD51*-foci positive and progressed under olaparib. This suggested that, despite severely reduced *BRCA1* protein expression, HR remained at least partially functional in these models, thus precluding their sensitivity to olaparib. We treated *BRCA1* deficient cell lines with olaparib and derived resistant variants. We observed increased *BRCA1* and *RAD51* foci formation in olaparib resistant variants. The data presented herein suggest that tumors with epigenetically silenced *BRCA1* that have been exposed to genotoxic treatment show poor response to olaparib and exhibit *BRCA1* and *RAD51* foci formation capacity compatible with HR proficiency. Our data, thus, suggest that olaparib may not be a good indication in tumors with epigenetically silenced *BRCA1* and supports the implementation of *BRCA1* and *RAD51* nuclear foci assay as functional read out of HR deficiency in TNBC.

Materials and methods

TNBC and HGSOc PDX models and in vivo treatment

TNBC and Ovarian cancer PDX models establishment was as described (36, 37). PDX models used are described in Table 1. The study was reviewed and approved by the ethics committees for animal experimentations of the University of Montpellier (CEEA-LR-12028). PDX models were established from fresh tumor fragments obtained from the Pathology Department at the Comprehensive Cancer Center of Montpellier (ICM) after

informed consent of the patients. Establishment of PDX models was reviewed and approved by the institutional review board. Approximately 50 mm³ PDX fragments were grafted subcutaneously into the flank of 3-4week old Swiss-nude female mice (Charles Rivers, Saint-Germain-sur-l'Arbresle, France). The present study comprised three experimental arms; vehicle, olaparib and Carboplatin (CBP) treatment comprising 6 to 8 mice per arm. When median tumor volume reached 100-150mm³, mice were randomly distributed in the two arms and treatment was started. Olaparib (Lynparza, AstraZeneca) was administered orally 5 times/week for 5 weeks at 100 mg/kg. CBP (Accord Healthcare, Middlesex, UK) was administered by intra-peritoneal (IP) injection twice per week for 4 weeks at 50 mg/kg CBP. At treatment end, mice were euthanized to collect tumor samples for further biochemical (RNA and proteins) or histological analyses. Some mice were kept for tumor volume monitoring.

MS-PCR

CpG methylation patterns at the *BRCA1* promoter were determined using the MS-PCR assay as previously described (28).

Array-CGH

For each PDX sample, the genomic profile was established by using aCGH onto high-resolution 4 × 180 K CGH-microarrays (SurePrint G3-Human CGH-Microarray, Agilent Technologies). Human female DNA was used as reference (G152A, Promega, Madison, WI, USA). Both experimental and analytic methods have been previously described (38). All probes for aCGH were mapped according to the Genome Reference Consortium Human Build 37 (CGCh37/Hg19; https://www.ncbi.nlm.nih.gov/assembly/GCF_000001405.13/). We used two different threshold values (log₂ ratio > 0.5 and 1.0) to distinguish low- (gain/) from high- (amplification) and (log₂ ratio < -0.3 and -1) to distinguish simple loss from deletion CAN (Copy Number Alterations), respectively. Percentage of altered genome was the number of

TABLE 1 Principal bio-clinical characteristics of the patient tumors from which the PDX models were derived.

PDX ID	BRCA1 Status	Cancer type	Grade or Stage	NACT	Type of NACT	response to NACT	RFS months	OS months
b1995	WT	TNBC	SBR III	No	NA	NA	>120	>120
b3804	WT	TNBC	SBR III	yes	Taxol+ avastin	Poor response	>120	>120
b3977	Me/Me	TNBC	SBR III	yes	FEC+T	refractory	5	9
b4122	Me/Me	TNBC	SBR III	No	NA	NA	>120	>120
15b0018	Me/Me	TNBC	SBR II	yes	FEC+T	Poor response	35	>60
15b1516	U/Me	TNBC	SBR III	yes	FEC+T	refractory	7	8
Tm168	Mut pS1524fs	TNBC	SBR III	No	NA	NA	3	7
o10047	Mut Del exon 8-13	HGSOc	Stage IV	No	NA	NA	>145	>145

WT, wild type; Me/Me both alleles methylated. U/Me hemi methylation. TNBC, triple negative breast cancer; HGSOc, High grade serous ovarian carcinoma.

NC, not communicated; NA, not applicable; NACT, neoadjuvant chemotherapy; FEC, Fluorouracil. Epirubicin. Cyclophosphamide; RFS, recurrence free survival; OS, Overall Survival.

probes above the threshold divided by the total number of probes for autosomal chromosomes.

Genetic instability and HRD scores

For each tumor, to evaluate genetic instability, we quantified the activity of the 17 copy number signatures described (20) with the R package CINSignatureQuantification.

For each tumor, a HRD score (HRDaCGH score), based on losses of heterozygosity (LOH), was calculated as previously described (39). A score ≥ 10 was considered as HRD-high. The percentage of genome altered was calculated as the sum of altered probes divided by the total number of probes after removing sexual chromosomes.

Next generation sequencing

Mutation profiles were established by using targeted-NGS panel of 559 genes commonly mutated in breast cancer (40). The list of genes targeted is available in the Supplementary Information. The sequence data were aligned to the human reference genome (UCSC hg19) using Burrows–Wheeler Aligner (41). Tumor samples were sequenced at an average depth of 851 \times (range, 520 to 1055) for the targeted regions. Bam files were processed as described (40). Single nucleotide variants (SNVs) calling was performed with a consensus approach using 8 variants callers for the SNV (FreeBayes) (42), HaplotypeCaller (43), LoFreq (44), Mutect2 (45), PISCES (46), Platypus (47), VarDict (48) and Varscan2 (49) and 10 variants callers for the indel (FreeBayes (42), HaplotypeCaller (43), LoFreq (44), Mutect2 (45), pindel (50), PISCES (46), Platypus (47), Scalpel (51), VarDict (48) and Varscan2 (49)). Variants called by less than 5 variants callers were filtered out. Then, the filtered variants were annotated with the Annotate Variation Software (ANNOVAR, version 2013-11-12). Known variants found in dbsnp129 and dbsnp137 with a variant allele frequency (VAF) superior to 1% (1000 G or ESP6500) were removed. Finally, low frequency SNVs and indels that were suspected to be false positives were systematically inspected with IGV version 2.3.32 (52, 53). Mutations were classified as “neutral” or “damaging” using the majority rule of predictor software (provided by dbnsfp: Sift, Polyphen2, LRT, MutationTaster, MutationAssessor, FATHMM, RadialSVM, LR) as previously described (54). A “recurrent” mutation, also called “hot spot”, was defined as being found more than 10 times in the Catalogue of Somatic Mutations in Cancer (COSMIC V68) database (<http://cancer.sanger.ac.uk/cosmic>).

RT qPCR

Total RNA was isolated from cell lines lysed in TRIzol (Invitrogen, Fisher Scientific, Illkirch-Graffenstaden, France), while PDX tumors were lysed using Lysing Matrix D (MP BiomedicalsTM, Doornveld, France). Subsequently, the RNA was extracted using the RNeasy Kit (Qiagen, Les Ulis, France) following

manufacturer instructions. cDNAs were synthesized from 1 μ g of total RNAs using random hexamers and SuperScript III Reverse transcription (Invitrogen, Fisher Scientific, Illkirch-Graffenstaden, France). Real-time qPCR was performed on a LightCycler 480 SW 1.5 apparatus (Roche, Meylan, France) with ONEGreen[®] FAST QPCR PREMIX (Ozyme, Saint Cyr l'Ecole, France) and designed human specific primers (Supplementary Table 1). Results were quantified with a standard curve generated by serial dilutions of a reference cDNA preparation. GAPDH transcripts were used for normalization. The fold change in gene expression was calculated as: Fold change = $2^{-\Delta\Delta CT}$.

Cell lines and CRISPR-Cas9 engineered mutants

SUM159 and SUM149 TNBC cell lines a generous gift from Dr S Ethier (MUSC, Charleston, SC), were maintained in Ham's F-12 medium (GibcoTM, Fisher Scientific, Illkirch-Graffenstaden, France) supplemented with 5% FBS, 10 μ g/ml insulin, 1 μ g/ml hydrocortisone and 1% Antibiotic-antimycotic (100X) (GibcoTM, Fisher Scientific, Illkirch-Graffenstaden, France). UWB1.289PT cell line was obtained from the American Type Culture Collection (ATCC) and maintained in the 50% RPMI-1640 (GibcoTM), 50% MEGM (MEGM Bullet Kit; CC-3150, Lonza, Basel, Switzerland) and supplemented with 3% FBS, 1% Antibiotic-antimycotic (100X) (GibcoTM, Fisher Scientific, Illkirch-Graffenstaden, France). HCC38 cell line was obtained from ATCC and maintained in RPMI-1640 supplemented with 10% FBS and 1% Antibiotic-antimycotic.

For CRISPR-Cas9 generation of KO clones, SUM159PT cells were first transduced with a plasmid vector containing doxycycline inducible lentiviral expression of SpCas9. Lentiviral transduction was performed on 70% confluent cell cultures. Viral particles were added in the fresh medium containing 8 μ g/ml polybrene. After 16h the medium was changed and 2 μ g/ml puromycin added for cell selection for at least 5 days. Next, the cells were transduced as described above with two lentiviral plasmid vectors for the expression of sgBRCA1 (kind gift from Yea-Lih Lin, IGH, Montpellier). After lentiviral transduction, cells were selected with 400 μ g/ml G418 for 10 days and Cas9 expression was induced by treating a population of cells with 1 μ g/ml of doxycycline for 6 days. The cells were then cloned and clones verified for the KO by Sanger sequencing and western blot. All cell lines and selected clones were genetically typed by Eurofins Genomics cell line authentication (Eurofins Genomics, Les Ulis).

Protein extraction and Western blotting

Protein extracts were prepared by lysing either tumor tissue or cell line pellets on ice for 30 min in Tris-HCl pH7.4 50mM, NaCl 100mM, NaF 50mM, β -glycerophosphate 40mM, EDTA 5mM, Triton X100 1%, Aprotinin 10mg/ml, PMSF 100mM, Leupeptin 1mM, Pepstatin 1mM, followed by a short centrifugation to pellet debris. Protein concentrations were measured using the BCA kit (Fisher Scientific, Illkirch-Graffenstaden, France) SDS-PAGE gel

electrophoresis was done on 30µg protein samples subsequently transferred onto nitrocellulose membranes (Amersham, Velizy-Villacoublay, France) and incubated overnight at 4°C with the primary antibody. Antibodies used are listed in a separate section. Membranes were then washed and incubated with the appropriate secondary antibody in 5% non-fat dry milk in PBST for 2h at room temperature and revealed by incubation with Chemiluminescent HRP Substrate (Sigma Aldrich, Saint Quentin Fallavier, France).

Immunofluorescence

For cell lines, cells were grown on 12mm diameter slides cover slips in 24 well-plate for 24h, then drugs were added at the predetermined IC50 concentration. After 24h drugs were washed off and cells prepared as described below. For tumor tissues, 6µm cryosections were prepared from OCT embedded deep frozen tissue and mounted on Fisherbrand™ Superfrost™ Plus Microscope Slides (Fisher Scientific, Illkirch-Graffenstaden, France) and stored at -80°C until used. Cells and tumor sections were sequentially subjected to mild extraction (0.4% Triton in PBS, 5min in cold), fixation (4% PFA diluted in PBS) and blockage/permeabilization (3% BSA + 0.2% Triton in PBS, 1 hour at room temperature), incubated overnight at 4°C with the primary antibody (diluted in 3% BSA + 0.2% Triton in PBS), then with the secondary antibody (diluted in 3% BSA + 0.2% Triton in PBS, 1h at room temperature). Between each step, slides were washed 3 times with PBS. Tumor cryosections were immersed 0.1% SBB (Sigma Aldrich, Saint Quentin Fallavier, France) and 70% ethanol for 20 minutes at room temperature to reduce tissue autofluorescence and subsequently washed three times for 5 minutes PBS with 0.02% Tween 20. Stained sections or cell were counterstained with DAPI (Fisher Scientific, Illkirch-Graffenstaden, France) to stain the nuclei and cover slips were mounted with MWL4-88 (Citifluor, CliniSciences, Nanterre, France) and stored at 4°C. Antibodies used are described in the Antibody section.

Immunofluorescence images were acquired using Zeiss microscope with a 63X-immersion oil lens and generated using Zeiss Blue software. RAD51, BRCA1, 53BP1 and γH2AX nuclear foci were scored using the CellProfiler image analysis software (version 2.2.0, Broad Institute). At least three biological replicates of each model (both vehicle- and olaparib-treated) were analyzed. Cells presenting >5 foci/nucleus for RAD51, BRCA1, 53BP1 or γH2AX were considered positive and tumors presenting >10% of positive cells were scored positive for the given marker.

Antibodies

Immunofluorescence; rabbit anti-RAD51 PC130 1:300 (Merck Millipore Sigma Aldrich, Saint Quentin Fallavier, France), rabbit anti-geminin 52508 1:200 (CST OZYME, Saint Cyr l'Ecole, France), mouse anti-BRCA1 sc-6954 1:100 (SCBT, Heidelberg, Germany), mouse anti-γ-H2AX (H2-3F4, kind gift from Dr. Mustapha Oulad-Abdelghani, MAB-IGBMC Illkirch-Graffenstaden, 1:4000), rabbit anti-53BP1 NB100-304 1:500 (Bio-technie LTD, Abington, UK).

Secondary antibodies; goat anti-mouse Alexa Fluor 488 (Abcam ab150113, 1:1000), goat anti-rabbit Alexa Fluor 555 ab150078 1:1000 (Abcam, Cambridge, UK).

Western blotting; BRCA1 9010 1:500 (CST OZYME, Saint Cyr l'Ecole, France), BRCA2 A303-434A 1:1000 (Bethyl OZYME, Saint Cyr l'Ecole, France), PARP1 WH0000142M1 1:1000 (Sigma Aldrich, Saint Quentin Fallavier, France), RAD51 8875, 1:1000 (CST OZYME, Saint Cyr l'Ecole, France) and alfa tubulin T9026 1:20000 (Sigma Aldrich, Saint Quentin Fallavier, France); secondary antibodies goat anti-mouse-HRP 70745 1:10000 (CST OZYME, Saint Cyr l'Ecole, France) and goat anti-rabbit-HRP 7076 1:10000 (CST OZYME, Saint Cyr l'Ecole, France).

Results

PDX models show variable response to olaparib

To test the relative sensitivity of TNBC with silenced *BRCA1* due to promoter hypermethylation (designated hereafter *BRCA1-Me*) to the PARP inhibitor olaparib and assess the impact of neoadjuvant treatment (NACT) on olaparib sensitivity, we selected 8 PDX models (7 TNBC and 1 High Grade Serous Ovarian Carcinoma) showing different *BRCA1* profiles. Our experimental PDX set comprised 2 *BRCA1* wild type (*BRCA1-WT*) TNBC (b1995, b3804), 4 *BRCA1-Me* TNBC (b3977, b4122, 15b1516, 15b0018) and 2 (1 TNBC and 1 HGSO) *BRCA1* mutated (*BRCA1-Mut*) models (tm168, o10047) (Table 1; Supplementary Figure 1). *BRCA1-Me* PDX models 15b1516, 15b0018 and b3977 were established from post-NACT residual tumors that had shown poor response to neoadjuvant treatment (Table 1; Supplementary Figure 1). The two *BRCA1-Mut* models (tm168, o10047) and the remaining *BRCA1-Me* model (b4122) were established from treatment naïve tumors. Hypermethylation of the *BRCA1* promoter region was determined in both the PDX models and the patient tumors using methylation specific PCR (MS-PCR). It is of note that no pre-treatment biopsy was available for the tumors that had undergone NACT, hence, *BRCA1* promoter methylation was determined after NACT on these tumor samples. Of the four *BRCA1-Me* PDX, 3 presented homozygous (Me/Me) methylation (15b0018, b3977, b4122) and 1 hemizygous (Me/U) methylation (15b1516) (Supplementary Figure 2).

PDX were grafted subcutaneously on Swiss-nude mice and olaparib was administered orally at 100 mg/kg, 5days per week for 5 weeks. In a parallel treatment group, mice received 50mg/kg Carboplatin (CBP) by intraperitoneal injection twice a week for 4 weeks, while the control group received daily the olaparib vehicle administered orally. Tumor volumes were measured twice a week. Three (tm168, b4122, o10047) of the 8 PDX showed disease stabilization or limited tumor size reduction under olaparib treatment, while the 5 other models (b3804, 15b0018, 15b1516, b1995, b3977) progressed (Figures 1A, B; Supplementary Figure 3A). Of the 3 olaparib responders, PDX tm168 and o10047 were *BRCA1-Mut* and b4122 was *BRCA1-Me*, but established from a treatment naïve tumor. The 3 other *BRCA1-Me* models (15b0018,

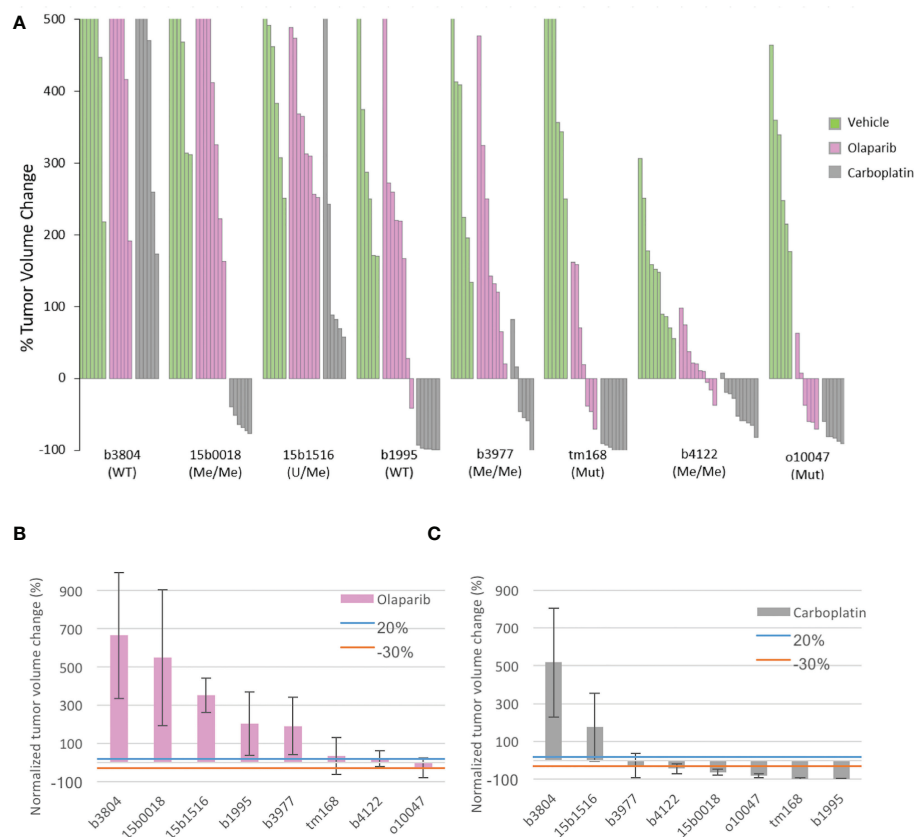


FIGURE 1
 Tumor volume change of the 8 PDX models under olaparib and Carboplatin treatment and principal characteristics related to HR of the PDX models (A) Waterfall plot of tumor volume changes in the 3 experimental arms were computed at the end of treatment for individual tumors as the percentage of the starting volume (green vehicle; pink olaparib, grey Carboplatin) (B) mean tumor volume change in each PDX model treated with olaparib. (C) mean tumor volume change in each PDX model treated with Carboplatin. Blue and orange lines indicate the +20% and -30% thresholds for tumor response defined by the RECIST criteria; > 20% progressive (PD), < 20% - > -30% stable disease (SD), < -30% responsive (R).

15b1516 and b3977, which progressed under olaparib, were established from tumors that had received NACT. In the CBP arms we globally noted more favorable response patterns, with 6 of 8 PDX models showing partial to complete response and 2 PDX (b3804, 15b1516) progressing under treatment (Figures 1A, C; Supplementary Figure 3A). Tumor growth was monitored after treatment end in 3 PDX, 2 *BRCA1-Me* TNBC (b3977, b4122) and 1 *BRCA1-Mut* HGSOc (o10047) (Supplementary Figure 3B) Both *BRCA1-Me* TNBC resumed growth shortly after end of olaparib administration. By contrast, the *BRCA1-Mut* o10047 exhibited complete regression 25 days after treatment ended and recurred after a lull of 3 weeks. In the CBP arm, progression after treatment end was observed in 1 of 3 PDX (b4122), while the two other models did not recur during the follow up period (Supplementary Figure 3B).

Genomic profiles and genetic instability scores of the tested TNBC models

Targeted sequencing was performed on the 7 TNBC PDX to search for mutations affecting principal DNA damage response genes and targetable cancer genes. The HGSOc PDX was analyzed by exome sequencing as part of a previous study (55). Mutations were

found in the *TP53*, *PTEN*, *KRAS*, *RIF1* and *STK11* genes (7, 2, 1, 1 and 1 PDX respectively) (Supplementary Table 2). No mutations were detected in further DNA repair genes such as *BRCA2*, *PALB2* or the *RAD51* orthologs *RAD51B*, *C* or *D*. The 8 PDX models were also analyzed for copy number changes by array-CGH. Genetic instability and HRD scores were determined (Figure 2A). All TNBC models, irrespective of *BRCA1* mutation or epigenetic silencing, presented elevated genetic instability scores (CX2, CX5) shown to be linked with *BRCA*-deficiency (20). We also noted that all tested TNBC models presented elevated HRD scores as defined by Abkevich and coworkers (39). Thus, elevated genetic instability and HRD scores suggested preexisting HR deficiency in the PDX models used in this study, including the two *BRCA1-WT* models.

We took advantage of the CGH analysis to determine copy number changes affecting key repair genes in the TNBC models. Except b3804, most PDX presented hemizygous losses affecting 3 to 4 HR genes of a list including *BRCA1*, *BRCA2*, *PALB2*, *RAD51*, *RAD51B* and *RAD51C* suggesting that the combined copy number reductions on these key HR genes could have contributed to a global HR attenuation and elevated genetic instability in these tumors (Supplementary Figure 4). But we cannot exclude the existence of undetected genetic or epigenetic anomalies affecting genes involved in HR maintenance.

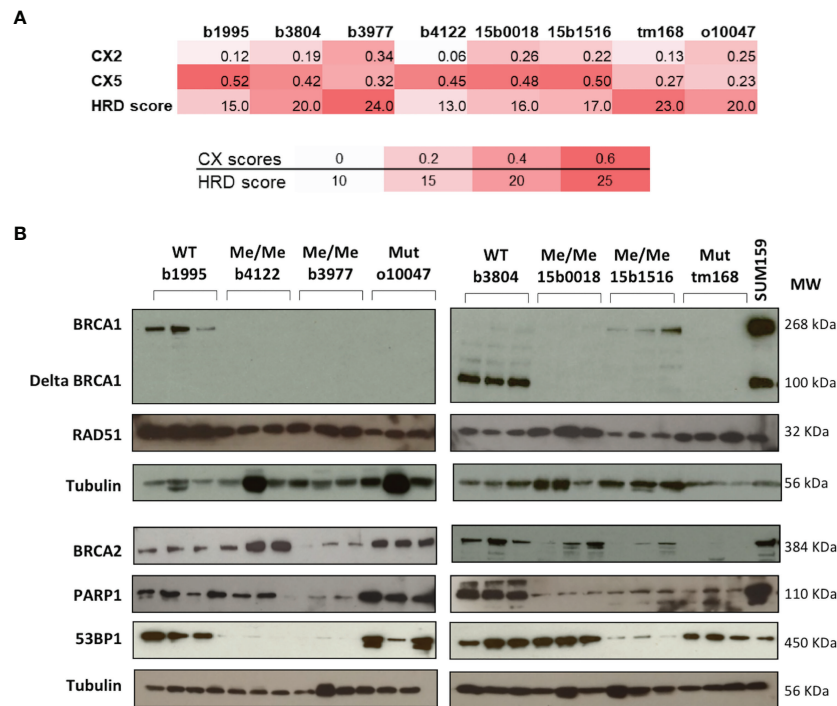


FIGURE 2
Principal characteristics related to HR of the PDX models. **(A)** CX Chromosomal instability and HRD scores of each PDX model. Color shades indicate from white to red the level of instability. **(B)** Protein expression patterns were assessed by Western blotting. The *BRCA1* status of each model is indicated on top of the autoradiograms. WT wild type. Me/Me homozygous methylation. U/Me hemizygous methylation. Mut coding mutation. For each PDX model three independent extracts from individual PDX tumors were loaded and analyzed. Proteins analyzed are indicated on the left and Molecular Weights in kDalton on the right. The protein extract of SUM159 cell line extract was added to the *BRCA1* panel to illustrate the full length and the $\Delta 11$ *BRCA1* protein variants.

Principal genes of the BRCA pathway showed protein expression profiles concordant with olaparib response

To determine the impact of promoter hypermethylation or coding mutations on *BRCA1* protein expression, *BRCA1* protein levels were measured by western blotting (WB) in the 8 PDX models. Noticeably, *BRCA1-Me* PDX b4122, b3977, 15b0018 and *BRCA1-Mut* o10047, tm168 showed no detectable *BRCA1* band, suggesting a loss of *BRCA1* functionality in these tumors. By contrast, the *BRCA1-WT* b1995, b3804 and the *BRCA1*-hemimethylated 15b1516 PDX presented detectable *BRCA1* bands (Figure 2B). We noted that PDX b3804 expressed high levels of a short 100 kD *BRCA1* protein isoform and low levels of the full length (268 kD) protein (Figure 2B). The 100 kD band is compatible with the size of the hypomorphic $\Delta 11$ -*BRCA1* isoform, which corresponds to a *BRCA1* splice-variant where exon 11 is excluded and that is frequently expressed in tumors bearing mutations in exon 11 (56). However, no *BRCA1* coding mutation, that could have explained the expression of the $\Delta 11$ -*BRCA1* isoform, was detected in PDX b3804 (Supplementary Table 1). We also analyzed expression of the *BRCA2*, *RAD51*, *PARP1* and *53BP1* proteins, which are important actors of HR. Whereas *RAD51* expression appeared elevated and relatively constant in the different PDX models, that of *BRCA2* was more variable, with no obvious link with *BRCA1* status or olaparib response, except

possibly the *BRCA1-Mut* PDX tm168, which showed very low *BRCA2* protein levels (Figure 2B). *PARP1* protein expression was detected in all PDX models, but, interestingly, the lowest levels were detected in the 3 *BRCA1-Me* (b3977, 150018 and 15b1516) that had been exposed to NACT and responded poorly to olaparib (Figure 1A). Finally, *53BP1* protein was expressed at high levels in 5 models and at low levels in 3 other PDX (Figure 2B).

BRCA1, RAD51 and 53BP1 nuclear foci formation in treated tumors correlate with olaparib response

In HR-proficient cells, *BRCA1* and *RAD51* proteins cluster at DNA damage sites forming nuclear foci that can be detected by immunofluorescence labeling. Absence of *BRCA1* and/or *RAD51* foci is considered as a sign of HR-deficiency. We scored the fraction of cells positive for *BRCA1* and *RAD51* foci in cryosections of PDX models sampled at the end of olaparib and vehicle treatment and searched for an association with olaparib response. Tumors presenting >10% cells showing >5 *BRCA1* or *RAD51* per nucleus were scored positive. PDX sections were immunolabeled with commercial antibodies directed against *BRCA1*, *RAD51*, and the S phase marker Geminin. Because of secondary antibodies species compatibility, *BRCA1* and *RAD51* were co-immunolabeled (Figure 3A; Supplementary Figure 5), whereas Geminin staining

was performed separately to ascertain the presence of S phase cells in each sample. Immunolabeling scoring was performed in 3 independent PDX tumors per model on at least 100 cells per section. Geminin staining showed 10 to 30% of Geminin-positive cells, confirming that tissue section actually comprised S phase tumor cells (Supplementary Figure 6). Four (4) of the 8 olaparib treated PDX, corresponding to 2 *BRCA1-Mut* (tm168, o10047) and 2 *BRCA1-Me* (b3977, b4122), scored negative for BRCA1-foci (Figures 3B, J), in agreement with the absence of BRCA1 band in the WB analysis (Figure 2B). BRCA1-foci positive models comprised two *BRCA1-WT* (b3804, b1995) and two *BRCA1-Me* PDX (b15b1516, 15b0018). Three of the four BRCA1-foci negative PDX (tm168, o10047, b4122) scored negative for RAD51-foci (Figures 3A, C, J, K) and corresponded to the 3 models that responded to olaparib (Figures 1A, B). Noticeably, PDX b3977, which progressed under olaparib (Figures 1A, B), scored positive for RAD51-foci, despite the fact it did not show BRCA1-foci (Figures 3A, C, J, K). All other RAD51-foci-positive PDX scored also positive for BRCA1 foci and showed mediocre response to olaparib (Figures 1A, B; 3A-C, J, K). Noticeably, the 3 *BRCA1-Me* models established from NACT treated TNBC (15b0018, 15b1516, b3977) were RAD51-foci positive and showed scores similar to those observed in the 2 *BRCA1-WT* models (b1995, b3804) (Figures 3B, J). By contrast, the *BRCA1-Me* PDX b4122, which was not exposed to NACT prior PDX establishment, was both BRCA1 and RAD51-foci-negative and did not progress under olaparib. These data suggested that while b4122 was indeed HR deficient, the 3 NACT treated *BRCA1-Me* models were, at least partially, HR proficient.

We verified whether BRCA1 or RAD51 nuclear foci formation was associated with olaparib response (Figures 3F-I). We noted a significantly association of BRCA1 and RAD51 foci absence (or low levels) with olaparib response (t-test $p=0.0017$ and $p<0.0001$ respectively) (Figures 3F, G). Interestingly, the differences in foci positive cells between responsive and non-responsive cells were discernible in both tumor sections from olaparib treated (Figures 3F, G) and sections from vehicle treated tumors and showed equivalent statistical significance (Figures 3J, K).

We also scored γ H2AX and 53BP1 foci, which are standard DNA damage markers, and observed that models presented 20 to 60% foci-positive cells for either marker, indicating severe DNA damage in olaparib treated PDX, to the exception of 15b1516 where only 5 to 10% cells scored positive (Figures 3D, E). Interestingly, we noted that 53BP1-foci tended to be more frequent in olaparib responsive PDX, compared with non-responsive PDX (t-test $p=0.028$) (Figure 3H). However, no difference was found with γ H2AX-foci (Figure 3I).

Acquired olaparib resistance in BRCA1 deficient cell lines is associated with increased BRCA1 and RAD51 foci formation and reduced levels of DNA damage

It is well documented that BRCA-deficient tumors or cell lines rapidly acquire resistance to treatment associated with the

restoration of HRR (56). We were, thus, interested to explore the restoration of RAD51-foci formation in *BRCA1*-deficient cell lines with acquired olaparib resistance. We, thus, isolated olaparib resistant clones from three cell lines; SUM159-KO1 and SUM159-KO2, two CRISPR *BRCA1* knock out clones we engineered from the TNBC SUM159 cell line, the SUM149 TNBC cell line which bears a frameshift mutation in exon 11 (2288delT) (57) and the UWB1.289 ovarian cancer cell line also showing a frameshift mutation in exon 11 (2594delC) (58). Resistance was obtained by exposing cell cultures to incremental olaparib concentrations for at least 12 weeks. Olaparib resistant cell lines were designated with the suffix Re (SUM159-KO1-Re, SUM159-KO2-Re, SUM149-Re and UWB1.289-Re). We characterized BRCA1, BRCA2, RAD51 and PARP1 protein expression by WB, as well as RNA expression changes associated with the acquisition of olaparib resistance (Figures 4A, B). In SUM159-KO1 and SUM159-KO2 no BRCA1 protein was detected. SUM159-KO1-Re reexpressed the full length BRCA1 protein and SUM159-KO2-Re showed no difference in BRCA1 protein expression compared with its clone of origin. SUM149 and UWB1.289 expressed no full length BRCA1 and variable levels of the Δ 11-BRCA1 100 kD band. Interestingly, SUM149-Re expressed the BRCA1 full length and increased levels of the Δ 11-BRCA1 variant, whereas UWB1.289-Re showed strongly increased Δ 11-BRCA1 levels (Figure 4A). No significant difference was found for BRCA2, RAD51 and PARP1 protein expression in the different cell line models. At the RNA expression level, we noted increased gene expression of *RAD51* and *RAD51C* in SUM159-KO1, of *RAD51C* and *ABCG2* in SUM149-Re, as well as of Δ 11-*BRCA1*, *RAD51C*, *RAD51D*, *PALB2* and *ATM* in UWB1.289-Re which could be related with their acquisition of olaparib resistance.

Next, we scored BRCA1, RAD51, 53BP1 and γ H2AX foci formation in the olaparib treated cell lines (Figure 5A). Except in SUM159-KO2-Re which does not express BRCA1, nor Δ 11-BRCA1, and scored BRCA1-foci-negative, BRCA1-foci scores tended to increase in olaparib resistant clones compared with cells of origin (Figure 5B). A similar trend was noticeable for RAD51-foci, whose numbers nearly doubled in olaparib resistant cells relative to cell lines of origin (Figure 5C). By contrast, 53BP1 and γ H2AX foci numbers clearly decreased in olaparib resistant variants (Figures 5D, E). These differences in foci numbers between olaparib resistant cells and their original counterparts, increase for BRCA1 and RAD51, decrease for 53BP1 and γ H2AX, were all statistically significant and in coherence with findings we made on PDX (Figures 5F-I). The reduction of γ H2AX-foci associated with the increase of BRCA1 and RAD51-foci observed in resistant cells suggest a global decrease of DNA damage in these cells upon olaparib treatment due to restored HR capacity. We also derived olaparib resistant cells from the hemimethylated *BRCA1-Me/UM* HCC38 TNBC cell line, whose methylation status we confirmed. While BRCA1-foci scores only modestly increased in olaparib treated cells, the fraction of RAD51-foci positive cells doubled in HCC38-Re variant cells (Supplementary Figure 7). Overall, our cell line data strongly support the notion that resistance to treatment and particularly to olaparib in BRCA1-deficient cancer cells is frequently associated with restoration of RAD51 foci formation, thus, signaling for restored HR capacity.

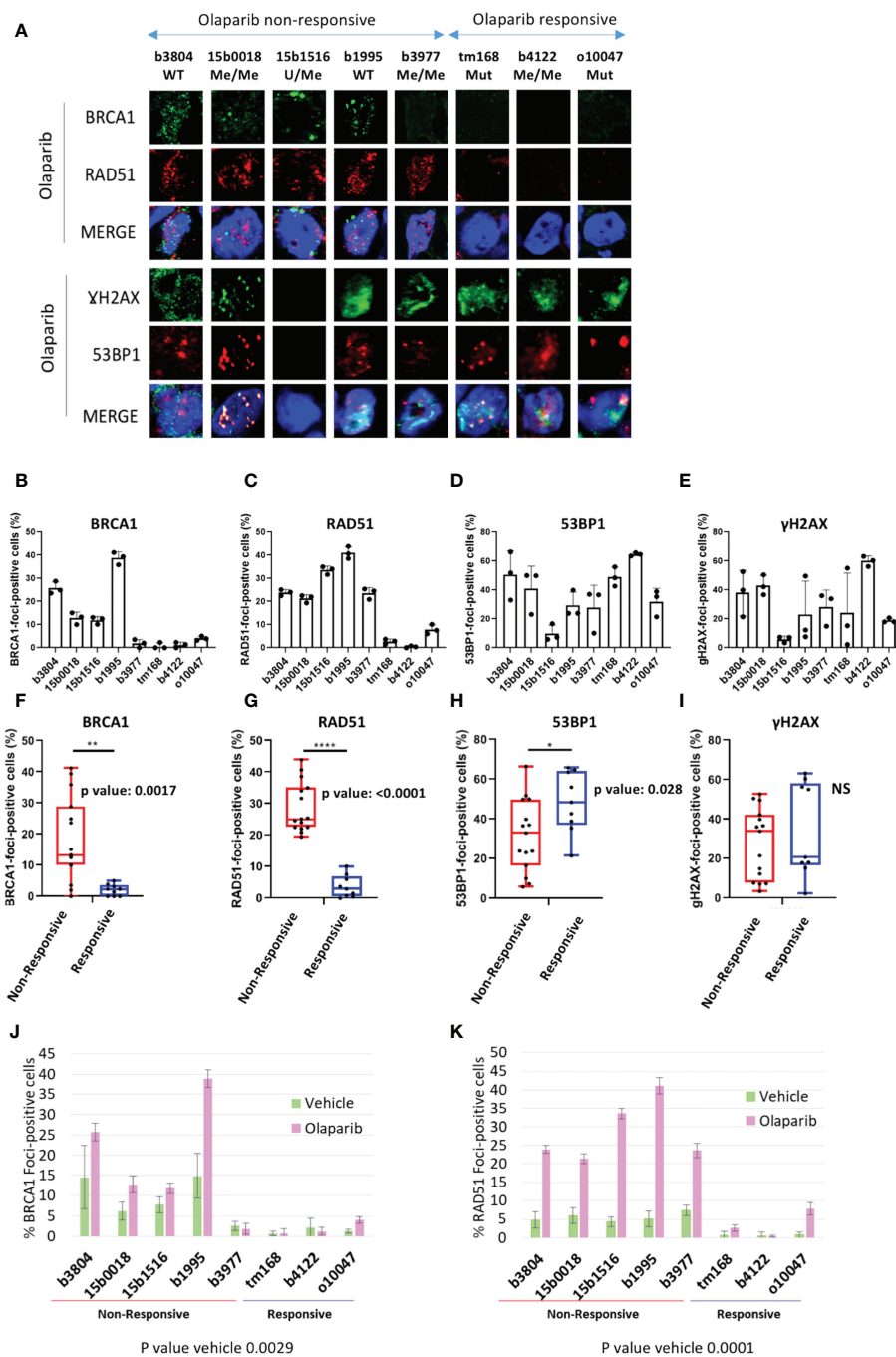


FIGURE 3

BRCA1, RAD51, γH2AX and 53BP1 nuclear foci formation in olaparib treated PDX. (A) Representative immunofluorescence images of frozen PDX tissue section harvested from mice sacrificed after the last administration of olaparib or before the tumor reached ethical size for vehicle treated models. PDX tumor sections were ordered from worst to best olaparib response. A complete version including vehicle treated tumors is visible in Supplementary Figure 5. (B) Quantification of BRCA1, (C) RAD51, (D) γH2AX, (E) 53BP1 foci formation in olaparib treated PDX. Results are represented as % of foci positive cells in the analyzed tumor sections in each PDX. Cells presenting at least 5 foci/nucleus were considered positive. At least 100 cells were quantified in each tissue section. (F–I) by two-tailed unpaired t-test analyses of correlation between foci numbers and olaparib response. Nuclear foci analyzed are indicated on top of each graph, as well as p-values. *, **, **** on top of the graph indicate the level of significance of the t-test (J, K) Histograms showing the percentage of BRCA1- (J) and RAD51- (K) foci positive cells of BRCA1 and RAD51 nuclear foci quantification in vehicle and olaparib treated PDX.

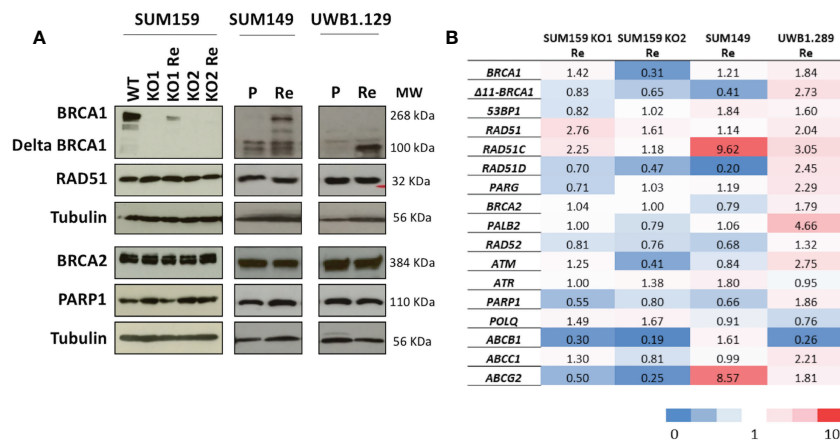


FIGURE 4

Protein and mRNA expression profiles of principal HR genes in the cell line models (A) Western blots showing protein expression patterns; analyzed proteins are indicated on the left and molecular weights in kDa on the right. (B) mRNA expression changes of genes potentially associated with olaparib resistance in cell line models selected for acquired olaparib resistance. mRNA levels are expressed as fold changes of the expression levels measured between the olaparib-resistant cell line and their parental lines used as reference (horizontal line). Reference cell lines were SUM159-KO1, SUM159-KO2 parental SUM149 and parental UWB1.289.

BRCA1, RAD51, γ H2AX and 53BP1 nuclear-foci as predictors of the response to olaparib or carboplatin

As PDX responding to CBP represented twice the number of olaparib responders (6 vs. 3 respectively), we wanted to determine whether the response to CBP was associated with reduced RAD51 and/or BRCA1-foci formation (Figures 1B, C). Like in the olaparib arm, individual grafts that responded to CBP were predominantly BRCA1-foci-negative/RAD51-foci-negative (Figures 6A, B) and, interestingly, most grafts of the BRCA-foci-negative/RAD51-foci-positive model b3977, whose response to olaparib was mediocre, showed tumor size reduction under CBP. However, grafts of the BRCA1-positive/RAD51-positive PDX 15b0018 and b1995, respectively *BRCA1-WT* and *BRCA1-Me* and bad responders to olaparib, showed good response to CBP pointing to the fact that CBP efficacy is not solely based on the HR status, but can also rely on alternative DNA repair mechanisms (Figure 6B). Despite these two BRCA1-foci-positive/RAD51-foci-positive models, both BRCA1-foci-negativity and RAD51-foci-negativity were significantly associated (t-test p-value 0.0059 and 0.0176 respectively) with CBP response in our dataset (Figure 6D). Next, we computed the Sensitivity, Specificity and Accuracy of RAD51, BRCA1, 53BP1 and γ H2AX foci in predicting the response to olaparib and CBP (Table 2). Concerning olaparib response RAD51 foci showed high sensitivity (88%), specificity (82%) and accuracy (84%), while BRCA1 foci showed excellent sensitivity (94%) but lower specificity (66%) and accuracy (74%). Interestingly, when CBP response was considered, BRCA1 foci performed globally better showing 70% sensitivity, 92% Specificity and 75% accuracy in comparison with RAD51 foci, which showed 57% sensitivity, 100% Specificity but 68% accuracy. The performances of 53BP1 and γ H2AX foci were overall rather contrasted showing excellent sensitivity (100%), but poor specificity (18%) and accuracy (41%) for olaparib response, while they reached better values for CBP response with high accuracy (87%) mitigating the mediocre specificity (46%). Overall,

these data support the use of RAD51 foci for olaparib response prediction, while BRCA1 foci, possibly in combination with RAD51 foci, appear interesting for CBP response. While γ H2AX and 53BP1 foci do not appear as convincing it may be interesting to reevaluate their performance for CBP response on a larger dataset.

Discussion

About one TNBC in three is estimated to be HR deficient. HRD has been linked with genetic or epigenetic impairment of genes belonging to the BRCA-pathway such as *BRCA1*, *BRCA2*, *PALB2* and *RAD51B*, *RAD51C* and *RAD51D*, but *BRCA1* is the most frequently affected gene in TNBC (5, 6). Because HR deficient tumors show increased sensitivity to PARPi or Platinum salts, detection of HRD has important implications in treatment definition (59). Identification of HRD is generally based on targeted sequencing of commonly mutated HR genes, combined with the determination of patterns of genomic rearrangements typical of HRD, such as the genomic HRD score, Tandem Duplication score or CX scores (20, 27, 31). However, BRCA-deficient cancers frequently develop resistance to treatment associated with HR restoration. Involved molecular events range from reverting secondary mutations, gene rearrangements producing gene chimeras, loss or mutations of the *53BP1* gene or of one of its cofactors in the Shieldin complex (34, 35, 59). Hence, the actual status of residual HRD tumors that have previously been exposed to genotoxic treatment could be in question. This point has been specifically raised concerning TNBC with silenced *BRCA1* gene due to hypermethylation of the promoter, whose sensitivity to PARPi has been disputed (31, 34).

These questions motivated the present study, where we interrogated the sensitivity to olaparib and CBP of 4 TNBC PDX models with epigenetically silenced *BRCA1*, 3 of which had received NACT prior PDX establishment. Noticeably, despite obliterated or severely reduced BRCA1 protein expression levels, the 3 *BRCA1*-

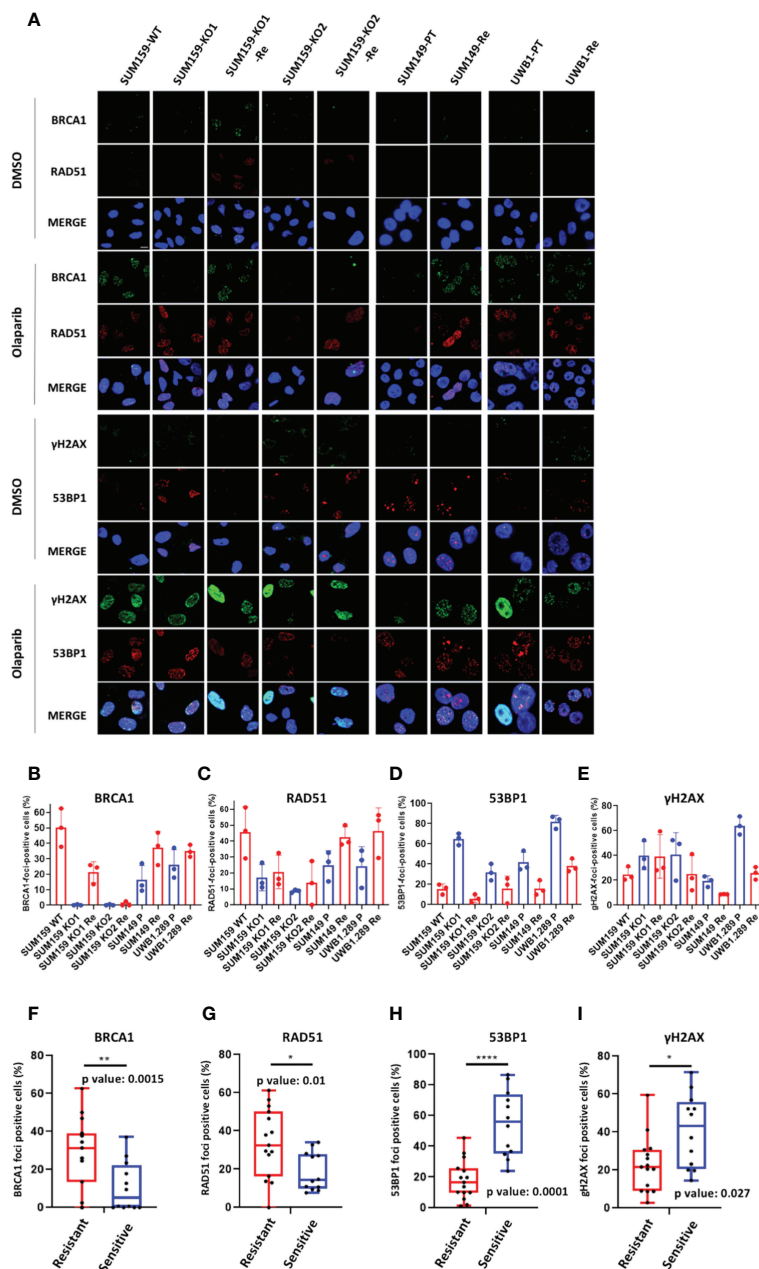


FIGURE 5

BRCA1, RAD51, γH2AX and 53BP1 nuclear foci in BRCA1 deficient cell line models (A) Representative immunofluorescence images of cell line models treated or not (control) with Olaparib for 24h. Cell line names are indicated on top *BRCA1*-WT (WT), *BRCA1*-KO (KO), *BRCA1*-KO-Ola-Resistant (Re), SUM149; parental (PT), Ola-Resistant (Re), UWB1.289; parental (PT), Ola-Resistant (Re) (B) BRCA1, (C) RAD51, (D) 53BP1, (E) γH2AX foci formation in the respective olaparib treated cell lines. Results are represented as % of foci positive cells in the analyzed tumor sections in each PDX. Cells presenting at least 5 foci/nucleus were considered positive. At least 150 cells were quantified in each section. Representative IF images are shown in the [Supplementary Figures](#). (F–I): Box plot presenting the difference in the number of BRCA1- (F), RAD51- (G), 53BP1- (H) and γH2AX- (I) foci positive cells between olaparib resistant and sensitive cell lines. p-values were calculated with two-tailed unpaired t-test. *, **, **** on top of the graph indicate the level of significance of the t-test

methyated PDX that had undergone NACT responded poorly to olaparib, showing response profiles similar to those of the two *BRCA1*-WT models used as controls. These observations, thus, questioned the actual functionality of HR in the *BRCA1*-Me PDX models included in our study, leading us to test for BRCA1 and RAD51 nuclear foci formation in tissue sections of olaparib treated PDX and use this assay as a functional read out. In HR proficient cells, the BRCA1 and RAD51 proteins cluster onto DNA lesions and

these clusters can be detected as nuclear foci by immunofluorescence microscopy (60). Their presence in tumor tissues signs for HR proficiency (61). Remarkably, the three *BRCA1*-Me PDX that responded poorly to olaparib scored positive for BRCA1 and/or RAD51 foci, likewise the two *BRCA1*-WT models. By contrast, the three PDX models responding to olaparib (2 *BRCA1*-Mut and 1 *BRCA1*-Me) scored negative for BRCA1 and RAD51-foci. Noticeably, the BRCA1 and RAD51 foci

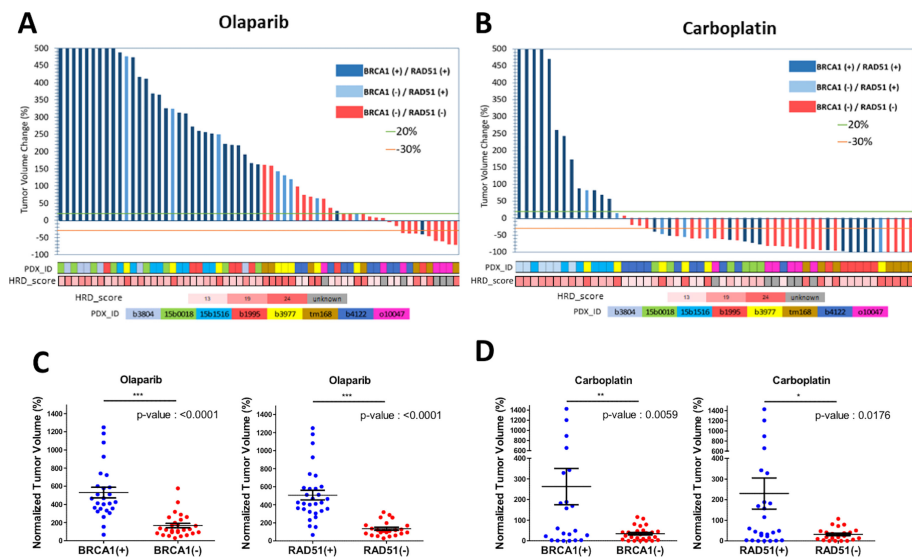


FIGURE 6
BRCA1 and RAD51 scores are good predictors of olaparib and Carboplatin response. Waterfall plots of the tumor volume change in individual PDX models (percentage of the starting volume) treated with either olaparib or Carboplatin. The status according to BRCA1 and/or RAD51 foci formation of each model is indicated by the color of the bar; dark blue BRCA1+/RAD51+; light blue BRCA1-/RAD51+; red BRCA1-/RAD51-. The identity of the PDX model is indicated by color boxes at the bottom of the graph. (A) olaparib treated mice. (B) Carboplatin treated mice. (C) tumor volume change under olaparib treatment stratified according to the BRCA1 foci status. (D) tumor volume change under olaparib treatment stratified according to the RAD51 foci status. *, **, *** on top of the graph indicate the level of significance of the t-test.

negative *BRCA1-Me* model had never been exposed to chemotherapy. Thus, our data suggest that HR was, at least partially, functional in the *BRCA1-Me* PDXs established from residual TNBC previously exposed to NACT, contributing to their poor response to olaparib. These observations were consistent with the increased RAD51 foci formation and HR restoration we evidenced in *BRCA1*-deficient cell line models that we rendered olaparib-resistant. Results presented herein support the notion that the actual HRD status of *BRCA1-Me* TNBC may be in doubt, especially if they have been previously exposed to genotoxic treatment. Since we did not have access to tumor samples

prior NACT, we cannot conclude on HR restoration due to treatment exposure, but our data are in line with previous reports (31, 35). This calls for the verification of the HRD status based on functional read outs such as BRCA1 and/or RAD51 foci formation (62). Indeed, genetic tests or genomic scores yield valuable information on the HRD status of a given tumor, however, they point to its natural history and may be misleading in terms of actual HR functionality. We wish, moreover, to point out that all the PDX models included in our study presented elevated HRD or genetic instability scores, irrespective of their mutational, *BRCA1* methylation status or sensitivity to olaparib.

TABLE 2 Test performance values for the indicated HRD biomarkers to predict olaparib and CBP response.

	Biomarkers	RAD51 Foci (n=61)	BRCA1 Foci (n=61)	γH2AX Foci (n=61)	53BP1 Foci (n=61)
Olaparib response	Sensitivity	88%	94%	100%	100%
	Specificity	82%	66%	18%	18%
	PPV	65%	52%	32%	32%
	NPV	95%	97%	100%	100%
	Accuracy	84%	74%	41%	41%
		(n=53)	(n=53)	(n=53)	(n=53)
CBP response	Sensitivity	57%	70%	100%	100%
	Specificity	100%	92%	46%	46%
	PPV	100%	97%	85%	85%
	NPV	43%	50%	100%	100%
	Accuracy	68%	75%	87%	87%

Response includes disease stabilization.

Genetic and genomic scores are being considered concurrently with RAD51 foci determination as biomarkers predictive of treatment in TNBC and prostate cancer (63–65). Results support the excellent correlation between low RAD51 scores and HR deficiency, as well as with increased sensitivity to olaparib or platinum based regimen (63, 65, 66). However, these works also point out the detection of tumors showing poor response to treatment, whilst presenting inactivating BRCA1 or BRCA2 mutations or elevated HRD scores and scoring positive for RAD51 foci. Our data are in perfect concordance with these observations and further support the relevance of BRCA1 and/or RAD51 foci-based tests to determine the functionality of HR in TNBC presenting all signs or HRD (63, 65, 66). Further, our data highlight the importance of verifying the actual functionality of HRR in tumors with epigenetically silenced *BRCA1*, particularly those previously exposed to chemotherapy during the course of the disease.

A number of studies highlight the exquisite sensitivity of HRD tumors to cis or carboplatin, alone or in combination with other molecules (63, 65, 66). We thus, documented the sensitivity to CBP of our models and determine their overlap with BRCA1 and RAD51 scores. PDX models responding to CBP were twice more frequent than olaparib responders and included all BRCA1-foci negative cases, as well as 2 BRCA1-foci/RAD51-foci positive PDX models, underlining the fact that CBP sensitivity is not solely determined by the HRD status. Indeed, platinum salts produces bulky adducts that must be removed by NER to avoid DNA breaks and tumors with faulty NER have been shown to be highly sensitive to platinum (59, 67, 68). Hence, while BRCA1 foci appeared a better predictor of CBP sensitivity than RAD51 in our dataset, they missed 2 out of 6 CBP sensitive cases, thus calling for complementary tests.

Conclusion

Our work shows that TNBC with a silenced *BRCA1* gene, due to hypermethylation of its promoter, may be prone to HR restoration and, thus, become resistant to olaparib. Interestingly, two of the olaparib resistant and RAD51-foci positive PDX models appeared sensitive to CBP. Our data thus support the notion that the HRD status of TNBC should be systematically checked using a combination of biomarkers, among which the BRCA1 and RAD51 foci formation tests play a major role. Not only do these assays inform on HR functionality in a given tumor, they are cheap, rapid and quite easy to implement. We performed the immunofluorescence analysis on olaparib treated tumor samples to ensure a clear signal difference between foci positive and foci negative samples, but noted, in accordance with other works, that the difference was also perceptible in non-treated tumors (63). Hence, this test, which we and others have shown to reliably predict sensitivity to olaparib, and also to CBP, could be implemented on Formalin fixed tumors as part of a pathology routine in a number of cancer treating institutions.

Data availability statement

The raw data supporting the conclusions of this article will be made available by the authors, without undue reservation.

Ethics statement

The animal study was reviewed and approved by CEEA-LR-12028.

Author contributions

Conceptualization: CT. Funding acquisition: WJ and CT. Investigation: CV, EO, IT, LF, JA, and EC. Methodology and resources: BO, MC, and AG. Supervision: CT and WJ. Validation: DB, CS, WJ, and CT. Writing: CT and WJ. All authors contributed to the article and approved the submitted version.

Funding

The authors declare that this study received funding from Astra-zeneca (contract # 2018-02069). The funder was not involved in the study design, collection, analysis, interpretation of data, the writing of this article, or the decision to submit it for publication. This work also benefited from the following financial support: Institut National du Cancer PRTK-2017 MODUREPOIS, Ligue Nationale Contre le Cancer 'Comité régional Occitanie-Est' 2021-R22031FF and the SIRIC Montpellier Cancer Grant INCa-DGOS-Inserm_12553.

Acknowledgments

The authors sincerely acknowledge Dr Genevieve Rodier for fruitful discussions and help throughout this project, Dr Isabelle Jariel for critical reading and constructive comments on the manuscript, and Dr Rui-Bras Gonçalves and Dr Stanislas du Manoir for help during the establishment of the PDX models. Furthermore, sincere thanks are due to the staffs of the animal facility at IRCM and the Centre de Ressources Biologiques at ICM for their constant support and expert help.

Conflict of interest

The authors declare that the research was conducted in the absence of any commercial or financial relationships that could be construed as a potential conflict of interest.

Publisher's note

All claims expressed in this article are solely those of the authors and do not necessarily represent those of their affiliated organizations, or those of the publisher, the editors and the reviewers. Any product that may be evaluated in this article, or claim that may be made by its manufacturer, is not guaranteed or endorsed by the publisher.

Supplementary material

The Supplementary Material for this article can be found online at: <https://www.frontiersin.org/articles/10.3389/fonc.2023.1125021/full#supplementary-material>

References

- Dent R, Trudeau M, Pritchard KI, Hanna WM, Kahn HK, Sawka CA, et al. Triple-negative breast cancer: clinical features and patterns of recurrence. *Clin Cancer Res* (2007) 13:4429–34. doi: 10.1158/1078-0432.CCR-06-3045
- Elias AD. Triple-negative breast cancer: A short review. *Am J Clin Oncol* (2010) 33:637–45. doi: 10.1097/COC.0b013e3181b8afcf
- Carey LA, Dees EC, Sawyer L, Gatti L, Moore DT, Collichio F, et al. The triple negative paradox: Primary tumor chemosensitivity of breast cancer subtypes. *Clin Cancer Res* (2007) 13:2329–34. doi: 10.1158/1078-0432.CCR-06-1109
- Zagami P, Carey LA. Triple negative breast cancer: Pitfalls and progress. *NPJ Breast Cancer*. (2022) 8:95. doi: 10.1038/s41523-022-00468-0
- Stephens PJ, Tarpey PS, Davies H, Van Loo P, Greenman C, Wedge DC, et al. The landscape of cancer genes and mutational processes in breast cancer. *Nature*. (2012) 486:400–4. doi: 10.1038/nature11017
- Couch FJ, Hart SN, Sharma P, Toland AE, Wang X, Miron P, et al. Inherited mutations in 17 breast cancer susceptibility genes among a Large triple-negative breast cancer cohort unselected for family history of breast cancer. *JCO*. (2015) 33:304–11. doi: 10.1200/JCO.2014.57.1414
- Lord CJ, Ashworth A. BRCAness revisited. *Nat Rev Cancer*. (2016) 16:110–20. doi: 10.1038/nrc.2015.21
- Roy R, Chun J, Powell SN. BRCA1 and BRCA2: different roles in a common pathway of genome protection. *Nat Rev Cancer*. (2012) 12:68–78. doi: 10.1038/nrc3181
- Helleday T, Eshtad S, Nik-Zainal S. Mechanisms underlying mutational signatures in human cancers. *Nat Rev Genet* (2014) 15:585–98. doi: 10.1038/nrg3729
- Hastak K, Alli E, Ford JM. Synergistic chemosensitivity of triple-negative breast cancer cell lines to Poly(ADP-ribose) polymerase inhibition, gemcitabine, and cisplatin. *Cancer Res* (2010) 70:7970–80. doi: 10.1158/0008-5472.CAN-09-4521
- Silver DP, Richardson AL, Eklund AC, Wang ZC, Szallasi Z, Li Q, et al. Efficacy of neoadjuvant cisplatin in triple-negative breast cancer. *J Clin Oncol* (2010) 28:1145–53. doi: 10.1200/JCO.2009.22.4725
- Sikov WM, Berry DA, Perou CM, Singh B, Cirincione CT, Tolaney SM, et al. Impact of the addition of carboplatin and/or bevacizumab to neoadjuvant once-per-week paclitaxel followed by dose-dense doxorubicin and cyclophosphamide on pathologic complete response rates in stage II to III triple-negative breast cancer: CALGB 40603 (Alliance). *J Clin Oncol* (2015) 33:13–21. doi: 10.1200/JCO.2014.57.0572
- Fong PC, Boss DS, Yap TA, Tutt A, Wu P, Mergui-Roelvink M, et al. Inhibition of poly(ADP-ribose) polymerase in tumors from BRCA mutation carriers. *N Engl J Med* (2009) 361:123–34. doi: 10.1056/NEJMoa0900212
- Tutt A, Robson M, Garber JE, Domchek SM, Audeh MW, Weitzel JN, et al. Oral poly(ADP-ribose) polymerase inhibitor olaparib in patients with BRCA1 or BRCA2 mutations and advanced breast cancer: a proof-of-concept trial. *Lancet* (2010) 376:235–44. doi: 10.1016/S0140-6736(10)60892-6
- Audeh MW, Carmichael J, Penson RT, Friedlander M, Powell B, Bell-McGuinn KM, et al. Oral poly(ADP-ribose) polymerase inhibitor olaparib in patients with BRCA1 or BRCA2 mutations and recurrent ovarian cancer: a proof-of-concept trial. *Lancet* (2010) 376:245–51. doi: 10.1016/S0140-6736(10)60893-8
- Robson M, Im S-A, Senkus E, Xu B, Domchek SM, Masuda N, et al. Olaparib for metastatic breast cancer in patients with a germline BRCA mutation. *N Engl J Med* (2017) 377:523–33. doi: 10.1056/NEJMoa1706450
- Davies H, Glodzik D, Morganello S, Yates LR, Staaf J, Zou X, et al. HRDetect is a predictor of BRCA1 and BRCA2 deficiency based on mutational signatures. *Nat Med* (2017) 23:517–25. doi: 10.1038/nm.4292
- Polak P, Kim J, Braunstein LZ, Karlic R, Haradhavala NJ, Tiao G, et al. A mutational signature reveals alterations underlying deficient homologous recombination repair in breast cancer. *Nat Genet* (2017) 49:1476–86. doi: 10.1038/ng.3934
- Menghi F, Barthel FP, Yadav V, Tang M, Ji B, Tang Z, et al. The tandem duplicator phenotype is a prevalent genome-wide cancer configuration driven by distinct gene mutations. *Cancer Cell* (2018) 34:197–210.e5. doi: 10.1016/j.ccell.2018.06.008
- Drews RM, Hernando B, Tarabichi M, Haase K, Lesluyes T, Smith PS, et al. A pan-cancer compendium of chromosomal instability. *Nature*. (2022) 606:976–83. doi: 10.1038/s41586-022-04789-9
- Glodzik D, Bosch A, Hartman J, Aine M, Vallon-Christersson J, Reuterswärd C, et al. Comprehensive molecular comparison of BRCA1 hypermethylated and BRCA1 mutated triple negative breast cancers. *Nat Commun* (2020) 11:3747. doi: 10.1038/s41467-020-18098-0
- Pujol P, Yaou K, Coffy A, Duforet-Frebourg N, Gabteni S, Daurès J-P, et al. Predominance of BRCA2 mutation and estrogen receptor positivity in unselected breast cancer with BRCA1 or BRCA2 mutation. *Cancers*. (2022) 14:3266. doi: 10.3390/cancers14133266
- Armstrong N, Ryder S, Forbes C, Ross J, Quek RG. A systematic review of the international prevalence of BRCA mutation in breast cancer. *CLEP* (2019) 11:543–61. doi: 10.2147/CLEP.S206949
- Telli ML, Timms KM, Reid J, Hennessy B, Mills GB, Jensen KC, et al. Homologous recombination deficiency (HRD) score predicts response to platinum-containing neoadjuvant chemotherapy in patients with triple-negative breast cancer. *Clin Cancer Res* (2016) 22:3764–73. doi: 10.1158/1078-0432.CCR-15-2477
- Tutt A, Tovey H, Cheang MCU, Kernaghan S, Kilburn L, Gazinska P, et al. Carboplatin in BRCA1/2-mutated and triple-negative breast cancer BRCAness subgroups: the TNT trial. *Nat Med* (2018) 24:628–37. doi: 10.1038/s41591-018-0009-7
- Staaf J, Glodzik D, Bosch A, Vallon-Christersson J, Reuterswärd C, Häkkinen J, et al. Whole-genome sequencing of triple-negative breast cancers in a population-based clinical study. *Nat Med* (2019) 25:1526–33. doi: 10.1038/s41591-019-0582-4
- Chopra N, Tovey H, Pearson A, Cutts R, Toms C, Proszek P, et al. Homologous recombination DNA repair deficiency and PARP inhibition activity in primary triple negative breast cancer. *Nat Commun* (2020) 11:2662. doi: 10.1038/s41467-020-16142-7
- Jacot W, Lopez-Crapez E, Mollevi C, Boissière-Michot F, Simony-Lafontaine J, Ho-Pun-Cheung A, et al. BRCA1 promoter hypermethylation is associated with good prognosis and chemosensitivity in triple-negative breast cancer. *Cancers*. (2020) 12:828. doi: 10.3390/cancers12040828
- Drew Y, Mulligan EA, Vong W-T, Thomas HD, Kahn S, Kyle S, et al. Therapeutic potential of poly(ADP-ribose) polymerase inhibitor AG014699 in human cancers with mutated or methylated BRCA1 or BRCA2. *J Natl Cancer Inst* (2011) 103:334–46. doi: 10.1093/jnci/djq509
- Veck J, Roperio S, Setien F, Gonzalez-Suarez E, Osorio A, Benitez J, et al. BRCA1 CpG island hypermethylation predicts sensitivity to poly(adenosine diphosphate)-ribose polymerase inhibitors. *J Clin Oncol* (2010) 28:e563–564. doi: 10.1200/JCO.2010.30.1010
- Menghi F, Banda K, Kumar P, Straub R, Dobrolecki L, Rodriguez IV, et al. Genomic and epigenomic BRCA alterations predict adaptive resistance and response to platinum-based therapy in patients with triple-negative breast and ovarian carcinomas. *Sci Transl Med* (2022) 14:eabn1926. doi: 10.1126/scitranslmed.abn1926
- Eikesdal HP, Yndestad S, Elzawahry A, Llop-Guevara A, Gilje B, Blix ES, et al. Olaparib monotherapy as primary treatment in unselected triple negative breast cancer. *Ann Oncol* (2021) 32:240–9. doi: 10.1016/j.annonc.2020.11.009
- D'Andrea AD. Mechanisms of PARP inhibitor sensitivity and resistance. *DNA Repair* (2018) 71:172–6. doi: 10.1016/j.dnarep.2018.08.021
- Dias MP, Moser SC, Ganesan S, Jonkers J. Understanding and overcoming resistance to PARP inhibitors in cancer therapy. *Nat Rev Clin Oncol* (2021) 18:773–91. doi: 10.1038/s41571-021-00532-x
- Ter Brugge P, Kristel P, van der Burg E, Boon U, de Maaker M, Lips E, et al. Mechanisms of therapy resistance in patient-derived xenograft models of BRCA1-deficient breast cancer. *J Natl Cancer Inst* (2016) 108:1–12. doi: 10.1093/jnci/djw148
- du Manoir S, Orsetti B, Bras-Gonçalves R, Nguyen T-T, Lasorsa L, Boissière F, et al. Ovarian carcinoma PDXs are genetically plastic and correspond to a subset of aggressive cancers prone to relapse. *Mol Oncol* (2014) 8:431–43. doi: 10.1016/j.molonc.2013.11.010
- Colombo P-E, du Manoir S, Orsetti B, Bras-Gonçalves R, Lambros MB, MacKay A, et al. Ovarian carcinoma patient derived xenografts reproduce their tumor of origin and preserve an oligoclonal structure. *Oncotarget*. (2015) 6:28327–40. doi: 10.18632/oncotarget.5069
- Adélaïde J, Finetti P, Bekhouche I, Repellini L, Geneix J, Sircoulomb F, et al. Integrated profiling of basal and luminal breast cancers. *Cancer Res* (2007) 67:11565–75. doi: 10.1158/0008-5472.CAN-07-2536
- Abkevich V, Timms KM, Hennessy BT, Potter J, Carey MS, Meyer LA, et al. Patterns of genomic loss of heterozygosity predict homologous recombination repair defects in epithelial ovarian cancer. *Br J Cancer*. (2012) 107:1776–82. doi: 10.1038/bjc.2012.451
- Bertucci F, Finetti P, Guille A, Adélaïde J, Garnier S, Carbuca N, et al. Comparative genomic analysis of primary tumors and metastases in breast cancer. *Oncotarget*. (2016) 7:27208–19. doi: 10.18632/oncotarget.8349
- Li H, Durbin R. Fast and accurate short read alignment with burrows-wheeler transform. *Bioinformatics*. (2009) 25:1754–60. doi: 10.1093/bioinformatics/btp324
- Garrison E, Marth G. Haplotype-based variant detection from short-read sequencing (2012). Available at: <https://arxiv.org/abs/1207.3907>.
- Poplin R, Ruano-Rubio V, DePristo MA, Fennell TJ, Carneiro MO, van der Auwera GA, et al. Scaling accurate genetic variant discovery to tens of thousands of samples. *bioRxiv* (2017). doi: 10.1101/201718
- Wilm A, Aw PPK, Bertrand D, Yeo GHT, Ong SH, Wong CH, et al. LoFreq: a sequence-quality aware, ultra-sensitive variant caller for uncovering cell-population heterogeneity from high-throughput sequencing datasets. *Nucleic Acids Res* (2012) 40:11189–201. doi: 10.1093/nar/gks918
- Auwera GAVd, O'Connor BD. *Genomics in the cloud: Using docker, GATK, and WDL in Terra*. O'Reilly Media (2020).
- Dunn T, Berry G, Emig-Agius D, Jiang Y, Lei S, Iyer A, et al. Pisces: an accurate and versatile variant caller for somatic and germline next-generation sequencing data. *Bioinformatics* (2019) 35:1579–81. doi: 10.1093/bioinformatics/bty849

47. Rimmer A, Phan H, Mathieson I, Iqbal Z, Twigg SRF, Wilkie AOM, et al. Integrating mapping-, assembly- and haplotype-based approaches for calling variants in clinical sequencing applications. *Nat Genet* (2014) 46:912–8. doi: 10.1038/ng.3036
48. Lai Z, Markovets A, Ahdesmaki M, Chapman B, Hofmann O, McEwen R, et al. VarDict: a novel and versatile variant caller for next-generation sequencing in cancer research. *Nucleic Acids Res* (2016) 44:e108–8. doi: 10.1093/nar/gkw227
49. Koboldt DC, Zhang Q, Larson DE, Shen D, McLellan MD, Lin L, et al. VarScan 2: Somatic mutation and copy number alteration discovery in cancer by exome sequencing. *Genome Res* (2012) 22:568–76. doi: 10.1101/gr.129684.111
50. Ye K, Schulz MH, Long Q, Apweiler R, Ning Z, Pindel: a pattern growth approach to detect break points of large deletions and medium sized insertions from paired-end short reads. *Bioinformatics*. (2009) 25:2865–71. doi: 10.1093/bioinformatics/btp394
51. Fang H, Bergmann EA, Arora K, Vacic V, Zody MC, Iossifov I, et al. Indel variant analysis of short-read sequencing data with scalpel. *Nat Protoc* (2016) 11:2529–48. doi: 10.1038/nprot.2016.150
52. Robinson JT, Thorvaldsdóttir H, Winckler W, Guttman M, Lander ES, Getz G, et al. Integrative genomics viewer. *Nat Biotechnol* (2011) 29:24–6. doi: 10.1038/nbt.1754
53. Thorvaldsdottir H, Robinson JT, Mesirov JP. Integrative genomics viewer (IGV): high-performance genomics data visualization and exploration. *Briefings Bioinf* (2013) 14:178–92. doi: 10.1093/bib/bbs017
54. Bertucci F, Rypens C, Finetti P, Guille A, Adélaïde J, Monneur A, et al. NOTCH and DNA repair pathways are more frequently targeted by genomic alterations in inflammatory than in non-inflammatory breast cancers. *Mol Oncol* (2020) 14:504–19. doi: 10.1002/1878-0261.12621
55. Manoir S, Delpech H, Orsetti B, Jacot W, Pirot N, Noel J, et al. In high-grade ovarian carcinoma, platinum-sensitive tumor recurrence and acquired-resistance derive from quiescent residual cancer cells that overexpress CRYAB, CEACAM6, and SOX2. *J Pathology*. (2022) 257:367–78. doi: 10.1002/path.5896
56. Wang Y, Bernhardt AJ, Cruz C, Kraus JJ, Nacson J, Nicolas E, et al. The BRCA1- $\Delta 11q$ alternative splice isoform bypasses germline mutations and promotes therapeutic resistance to PARP inhibition and cisplatin. *Cancer Res* (2016) 76:2778–90. doi: 10.1158/0008-5472.CAN-16-0186
57. Elstrodt F, Hollestelle A, Nagel JHA, Gorin M, Wasielewski M, van den Ouweland A, et al. BRCA1 mutation analysis of 41 human breast cancer cell lines reveals three new deleterious mutants. *Cancer Res* (2006) 66:41–5. doi: 10.1158/0008-5472.CAN-05-2853
58. DelloRusso C, Welch PL, Wang W, Garcia RL, King M-C, Swisher EM. Functional characterization of a novel BRCA1-null ovarian cancer cell line in response to ionizing radiation. *Mol Cancer Res* (2007) 5:35–45. doi: 10.1158/1541-7786.MCR-06-0234
59. Konstantinopoulos PA, Ceccaldi R, Shapiro GI, D'Andrea AD. Homologous recombination deficiency: Exploiting the fundamental vulnerability of ovarian cancer. *Cancer Discovery*. (2015) 5:1137–54. doi: 10.1158/2159-8290.CD-15-0714
60. Willers H, Taghian AG, Luo C-M, Treszezamsky A, Sgroi DC, Powell SN. Utility of DNA repair protein foci for the detection of putative BRCA1 pathway defects in breast cancer biopsies. *Mol Cancer Res* (2009) 7:1304–9. doi: 10.1158/1541-7786.MCR-09-0149
61. Graeser M, McCarthy A, Lord CJ, Savage K, Hills M, Salter J, et al. A marker of homologous recombination predicts pathologic complete response to neoadjuvant chemotherapy in primary breast cancer. *Clin Cancer Res* (2010) 16:6159–68. doi: 10.1158/1078-0432.CCR-10-1027
62. van Wijk LM, Kramer CJH, Vermeulen S, ter Haar NT, de Jonge MM, Kroep JR, et al. The RAD51-FFPE test; calibration of a functional homologous recombination deficiency test on diagnostic endometrial and ovarian tumor blocks. *Cancers*. (2021) 13:2994. doi: 10.3390/cancers13122994
63. Castroviejo-Bermejo M, Cruz C, Llop-Guevara A, Gutiérrez-Enríquez S, Ducy M, Ibrahim YH, et al. A RAD 51 assay feasible in routine tumor samples calls PARP inhibitor response beyond BRCA mutation. *EMBO Mol Med* (2018) 10:1–16. doi: 10.15252/emmm.201809172
64. Carreira S, Porta N, Arce-Gallego S, Seed G, Llop-Guevara A, Bianchini D, et al. Biomarkers associating with PARP inhibitor benefit in prostate cancer in the TOPARP-b trial. *Cancer Discovery*. (2021) 11:2812–27. doi: 10.1158/2159-8290.CD-21-0007
65. Pellegrino B, Herencia-Ropero A, Llop-Guevara A, Pedretti F, Moles-Fernández A, Viaplana C, et al. Preclinical *In vivo* validation of the RAD51 test for identification of homologous recombination-deficient tumors and patient stratification. *Cancer Res* (2022) 82:1646–57. doi: 10.1158/0008-5472.CAN-21-2409
66. Llop-Guevara A, Loibl S, Villacampa G, Vladimirova V, Schneeweiss A, Karn T, et al. Association of RAD51 with homologous recombination deficiency (HRD) and clinical outcomes in untreated triple-negative breast cancer (TNBC): analysis of the GeparSixto randomized clinical trial. *Ann Oncol* (2021) 32:1590–6. doi: 10.1016/j.annonc.2021.09.003
67. Reardon JT, Vaisman A, Chaney SG, Sancar A. Efficient nucleotide excision repair of cisplatin, oxaliplatin, and bis-aceto-amine-dichloro-cyclohexylamine-platinum(IV) (JM216) platinum intrastrand DNA diadducts. *Cancer Res* (1999) 59:3968–71.
68. Ceccaldi R, O'Connor KW, Mouw KW, Li AY, Matulonis UA, D'Andrea AD, et al. A unique subset of epithelial ovarian cancers with platinum sensitivity and PARP inhibitor resistance. *Cancer Res* (2015) 75:628–34. doi: 10.1158/0008-5472.CAN-14-2593